AIAA JOURNAL
Vol. 36, No. 3, March 1998

Free- and Near-Free-Surface Swirling Turbulent Jets

M. S. Feyedelem* and T. Sarpkaya†
U.S. Naval Postgraduate School, Monterey, California 93943

The turbulent flowfield created by a round swirling jet issuing from a nozzle, beneath and parallel to a free surface, in both the deep- and shallow-submergence modes has been studied for three swirl numbers (S = 0.265, 0.500, and 0.522) and fixed Froude and Reynolds numbers using a three-component laser Doppler velocimetry system. The results have shown that a swirling jet is unique among all shear flows; stagnation occurs without vortex breakdown at a critical swirl of S = 0.50; vortex breakdown occurs for $S \geq 0.51$ and leads to the intensification of turbulence within or near the exit of the nozzle and to the nonmonotonic change of the turbulent kinetic energy with S; turbulence shear stresses exhibit anisotropic behavior, especially in the plane bisecting the jet; and the degree of anisotropy at the free surface depends on the degree of agitation of the free surface (swirl number, Froude number, x/d, and Reynolds number). The need for a robust turbulence model that can deal with the alteration of turbulence by distortion and rotation is emphasized.

Nomenclature

a	= normalized distance to virtual origin
d	= nozzle exit diameter
F	= Froude number, $U_o/\sqrt{gh}$
G_x	= axial flux of axial momentum
G_θ	= axial flux of angular momentum
g	= gravitational acceleration
h	= depth of nozzle axis from free surface
Re	= Reynolds number, $U_o d/\nu$
S	= swirl number
U	= velocity
U_m	= maximum velocity u at a given x/d
U_o	= mean nozzle exit velocity
u, v, w	= axial, transverse (tangential), and vertical (radial) velocity components, respectively
u', v', w'	= rms of fluctuating axial, tangential, and radial velocity components
$u'w'$	= temporal mean of a Reynolds shear stress
V_m	= maximum tangential velocity at a given x/d
x	= axial coordinate, origin at nozzle exit
x^*	= $x/(x + ad)$
y	= lateral coordinate
z	= vertical coordinate, origin on x axis
z^*	= $z/(x + ad)$
Γ	= circulation of vortex
ν	= kinematic viscosity
ρ	= density of fluid

Introduction

THE current impetus for research on both the free- and near-free-surface swirling jets comes, in part, from the need to monitor and/or reduce the remotely sensible signatures created on the free surface by submerged and surface maritime traffic,[1,2] to understand the mutual interaction between the structure of the underlying turbulence and the free surface disturbances,[3] to enhance mixing in combustion chambers,[4,5] to increase the ratio of the heat transfer to the required pumping power, to develop active shear-layer control with swirl,[6] to precipitate the destruction of trailing vortices,[7–9] and to contribute to flow physics and numerical simulations. The unifying feature of these swirling flows (with or without free-surface or wall-proximity effects) is that their behavior is determined more by streamline curvature, centrifugal acceleration, and turbulent transport than by pressure effects. Also, they provide ideal benchmark tests for turbulence closures. The numerical experiments with free swirling jets have highlighted defects in nearly all current closure models.[10–17] The predictions were somewhat improved only when the optimum values of the modeling parameters were extracted from the data simulated (one physics/one model situation). All model makers have expressed the strong need for more experimental data for a better understanding of the effects of swirl on turbulence models. This is particularly critical for swirling flows interacting with a free surface.[3]

There are a number of studies closely related to the present investigation.[18–24] They have been carried out with fully submerged free or confined swirling jets. They have uniformly concluded that the characteristics of swirling flows are highly complex for they depend partly on the preexit history of the flow within the nozzle and partly on the postexit circumstances surrounding the jet. In fact, there are no precise means to characterize the degree of swirl imparted to a flow because of the strong influence of the nozzle conditions. Among the numerous proposals, the one most widely used is the swirl number S, defined by Chigier and Chervinsky[18] as

$$S = \frac{G_\theta}{G_x(d/2)} \tag{1}$$

where $d/2$ is the equivalent nozzle radius; G_θ is given by

$$G_\theta = \int_0^\infty (\rho uv + \rho u'v')r^2\,\mathrm{d}r \tag{2}$$

and G_x is given by

$$G_x = \rho \int_0^\infty \left[u^2 + u'^2 - \frac{1}{2}(v^2 + v'^2 + w'^2)\right] r\,\mathrm{d}r \tag{3}$$

The terms G_θ and G_x are the invariants of a given jet. In the present investigation, S was calculated as exactly as possible, for the nozzle tested, through the use of Eqs. (1–3). Furthermore, the integral invariants of the jet were examined in all test sections to assess the internal consistency of the measurements.

It is a widely recognized fact that the swirl number S is insufficient to uniquely describe the character of swirling flows.[18–24] Thus, the evolution of a robust turbulence model that would consistently account for the effects of streamline curvature, centrifugal acceleration, and free-surface proximity, without resorting to case-specific modeling parameters, needs well-executed experiments with the same nozzle in both the fully submerged and near-free-surface conditions. As its primary objective, the present investigation deals first with swirling turbulent liquid jets, discharging into a large medium of water (to create an extensive and detailed reference database) and, subsequently, with identical swirling jets running beneath and parallel to a free surface. There are no previous studies of the interaction of a swirling jet with a free surface.

Presented as Paper 97-0438 at the AIAA 35th Aerospace Sciences Meeting and Exhibit, Reno, NV, Jan. 6–10, 1997; received Jan. 16, 1997; revision received Sept. 29, 1997; accepted for publication Nov. 15, 1997.

*Lieutenant, U.S. Navy.
†Distinguished Professor, Department of Mechanical Engineering. Associate Fellow AIAA.

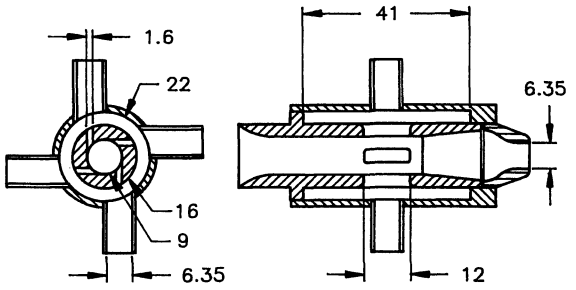

Fig. 1 Axial-plus-tangential-entry swirl generator (dimensions in millimeters).

Experimental Facility

The experiments were conducted in an existing recirculating free-surface water tunnel (about 8 m^3). The open test section was 50 cm wide, 50 cm deep, and about 6 m long. During the off-test periods, a small pump continuously filtered the tunnel water through a microfiltration system to remove rust and other suspended fine particles, down to about 10 μm, from the water.

An axial-plus-tangential-entry swirl generator (Fig. 1) with a converging nozzle similar but not identical to that devised by Chigier and Chervinsky[18] was used. The axial and tangential flow into the nozzle were controlled and measured independently and monitored continuously with two calibrated rotameters.

A conical receiver (about one-third the size of the tunnel cross section) was placed 3 m downstream from the nozzle to collect and to recirculate the flow (as well as the scattering particles, as noted later) through the pumps independently controlling the axial and tangential flows. Thus, only the entrained fluid had to recirculate along the remainder of the tunnel with a cross-sectional mean velocity of about 0.35 mm/s. The sides of the nozzle were free, and the entrainment was not constrained as in the case of wall jets.

The mean velocities and turbulence intensities were measured with a three-component laser Doppler anemometer (Dantec) and a 10-W coherent laser system, first configured for backward scattering and then for forward scattering. Bragg cells were used to shift the frequency of one beam of each pair by 40 MHz to provide directional sensitivity and to prevent fringe bias. The crossing of the six beams was achieved using a 50-μm pinhole and the built-in beam steerers. The probe volume (approximately 50 μm in diameter and about 150 μm in length) was positioned at the required location by use of an automated, computer-controlled x-y-z traversing mechanism. The positioning of the probe volume was found to be ± 1 step of the stepper motor, which has a resolution of 100 steps/mm. Very small quantities of light-scattering particles (5 μm round Polyamid particles of specific gravity of 1.01) were introduced into the return line from the conical receiver after being continuously stirred in a large plastic container. No data were collected during the startup period (at least 1 h) of the operation of the system during which the count rate of bursts in coincidence mode reached at least 2 kHz, with a validation rate of 96–100%. At least 10,000 samples for the calculation of statistical moments and 10^6 samples for the spectra were collected at each measurement location. The digital outputs of the counterprocessors were fed into a data acquisition system. The statistical parameters derived from these measurements are subject to biases from several sources, particularly in regions of high turbulence intensity, and there is not yet a generally accepted proper correction procedure. In this work, the velocity bias, the most significant of all the biases, was corrected using the approaches described by Stevenson et al.[25] and McLaughlin and Tiederman.[26] The two approaches yielded nearly identical results for turbulence intensities below about 20%.

The measurements for the three mean velocity and the six turbulent stress-tensor components were made in a free swirling jet at $x/d = 0.14$ [$x = 0.88$ mm, the minimum x at which laser Doppler velocimetry (LDV) measurements can be made], 1, 2, 3, 4, 5, 7, 10, 16, and 32. For the near-free-surface case, the nozzle axis was placed at $h = 3.5d$ from the undisturbed free surface, and the measurements were made at $x/d = 0.14$, 0.5, 2, 4, 6, 8, 10, 12, 16, and 32. At each section, all velocity and turbulence quantities were measured along the vertical z axis and along the lateral y axis. In addition to the foregoing, a number of measurements were made very near the free surface, along the lines parallel to the y axis at $x/d = 10$. Finally, detailed velocity and turbulence measurements were made in both modes at four upstream sections near the nozzle ($x/d = 0.28$, 0.42, 0.56, and 0.70), to complement those already made at $x/d = 0.14$, to define the initial conditions, including the dissipation rate, as precisely as possible.

Every precaution was taken, and a conscientious effort was made to obtain archival quality data for use in the validation of numerical simulations. The uncertainties associated with the measurements were evaluated using the procedures suggested by Moffat.[27] The possible sources of error are power fluctuations, mistracking of the particles, temperature changes in the laboratory that affect the positioning of the traversing system, changes from the dam water to well water, the reading of the flow meters, occasional minor tremors, etc. The error in the velocity measurements is a function of the turbulence intensity, which varies considerably across the jet section. Nevertheless, it suffices to note that all of the experimental conditions could be repeated to a precision closer than $\pm 1\%$. On the average, uncertainties in mean velocities are $\pm 2\%$, in axial normal stresses of turbulence $\pm 3\%$, and in turbulent shear stresses $\pm 4\%$. To establish the repeatability of the procedures and data, each profile was measured at least twice at different times in both the forward- and backward-scattering modes (some, 12 months apart). The largest difference between the corresponding profiles was smaller than 2%.

Presentation and Discussion of Results

General Comments

The velocities u, v, and w represent the axial (along x), tangential (along y), and radial (along z) components. The bold symbols such as $\boldsymbol{u'}$ and $\boldsymbol{u'w'}$ denote $\sqrt{(u'^2)}$ and $\overline{u'w'}$, respectively. The mean velocities and the rms values of the fluctuating quantities were normalized by U_0 (the cross-sectional mean velocity at the nozzle exit), U_m (the maximum axial velocity), or V_m (the maximum tangential velocity) in a given distribution, along a given line, at a prescribed section to bring out the special features of the velocity profiles.

The distances along the x axis are measured either from the nozzle exit ($x = 0$) or from the virtual origin ($x = -ad$). As in Ref. 18, the value of a was determined by extrapolating lines of $1/U_m$ against x to the value of $1/U_m = 0$. Then x and z were normalized by $x + ad$, with $a = 3$, so that $x^* = x/(x + ad)$ and $z^* = z/(x + ad)$. Normally, a distinction has to be made between the actual jet axis and the x axis. The wakes of single-screw ships and submarines drift to the right or left depending on the direction of rotation of the propeller because of the swirl-induced momentum. The magnitude of the drift depends on the axial momentum of the flow. In the present investigation, U_o was 2.79 m/s [corresponding to a Reynolds number of $Re = U_o d/\nu = 1.8 \times 10^4$ and a Froude number of $F = U_o/\sqrt{(gh)} = 6$] and the drift was negligible (about $0.04d$) within a distance of $50d$ and certainly much smaller than the deflection of the jet axis toward the free surface (because of its mutual interaction with its image). For the sake of consistency, all velocity and turbulence plots were made relative to the x axis (the ideal center of the jet) rather than the local center of the jet. Figure 2

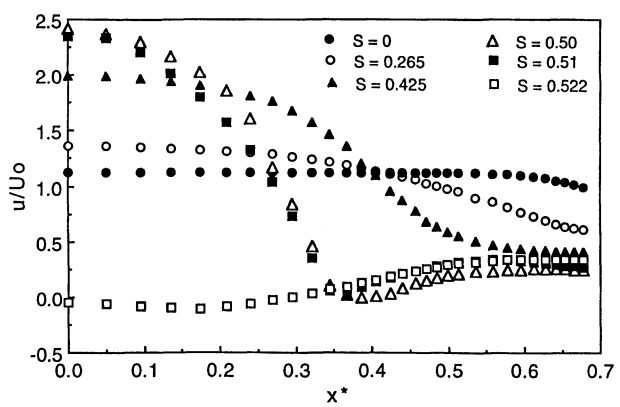

Fig. 2 Axial velocity u/U_o vs x^* for various swirl numbers S (deep mode).

shows u/U_o as a function of x^* in terms of six S values. For the subcritical value of $S = 0.265$, the decay is mainly due to the centrifugal expansion of the jet. For the critical value of $S = 0.50$, the rapid decrease to nearly zero and the subsequent increase to about $0.3U_0$ of the axial velocity shows that stagnation without vortex breakdown is achievable (see plots of $S = 0.50$ and 0.51). For the supercritical value of $S = 0.522$, the axial velocity reverses and vortex breakdown occurs.[28,29] Farokhi et al.[19] noted that their swirling jet has been brought to the point of breakdown at a swirl number of 0.48, significantly lower than the commonly assumed value of 0.6 but in near agreement with that found in the present investigation with a considerably different swirl generator. It is on the basis of this figure that three representative S values were chosen ($S = 0.265$, 0.500, and 0.522; mild, critical, and strong swirl, respectively) for the detailed measurement of the mean velocities and Reynolds stresses at numerous sections. This led to an overwhelming number of data points and plots. Here only a small fraction of the data could be presented because of space limitations. All of the data, including those at other h/d values, will be available for computational fluid dynamics simulations. Our modeling efforts will be the subject of a separate paper.

Case of a Swirling Jet with $S = 0.265$

Figures 3 and 4 show the axial and swirl velocities u/U_m and v/U_m as a function of z^* for $S = 0.265$. One data set is for the fully submerged free swirling jet (deep mode or DM), and the other for the same jet whose axis is at a distance of $h = 3.5d$ from the undisturbed, clean, free surface (shallow mode or SM). These data were obtained at $x/d = 0.14$ ($x = 0.88$ mm) to establish the upstream conditions. The excellent agreement between the two sets of data for both u/U_m and v/U_m shows that there are no free-surface effects on the mean velocities at $x/d = 0.14$. However, this is not the case for the fluctuations of the swirl component of the velocity, as will be seen later.

The evolution of u/U_m, v/U_m, u'/U_0, v'/U_0, and $u'w'/U_o^2$ for the deep mode alone are shown in Figs. 5–9 at various axial stations. Figure 5 shows that the contraction of the nozzle increases the maximum velocity at the axis, and the profile becomes more top hat like.[30]

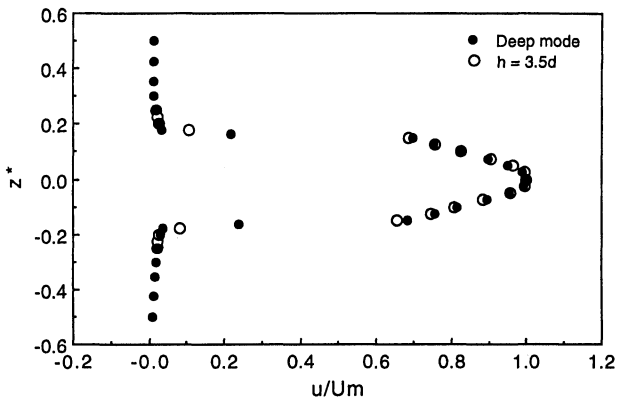

Fig. 3 Axial velocity u/U_m vs z^* at $x/d = 0.14$ for $S = 0.265$ (deep and shallow modes).

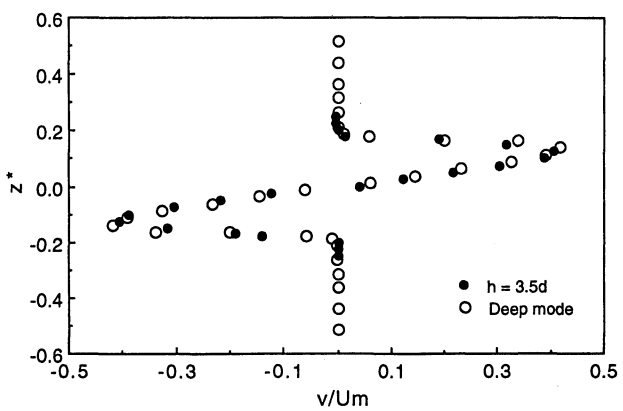

Fig. 4 Tangential velocity v/U_m vs z^* at $x/d = 0.14$ for $S = 0.265$ (deep and shallow modes).

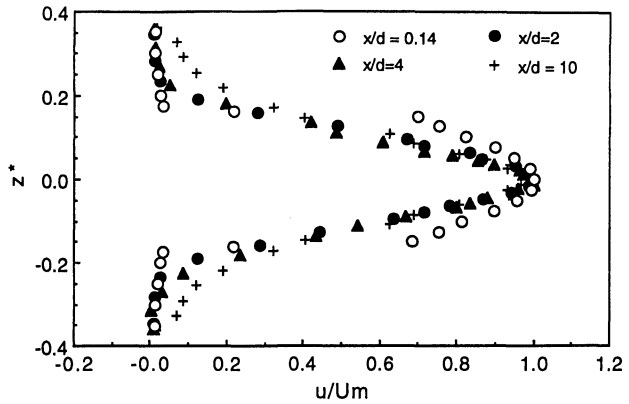

Fig. 5 Axial velocity u/U_m vs z^* at four x/d values for $S = 0.265$ (deep mode).

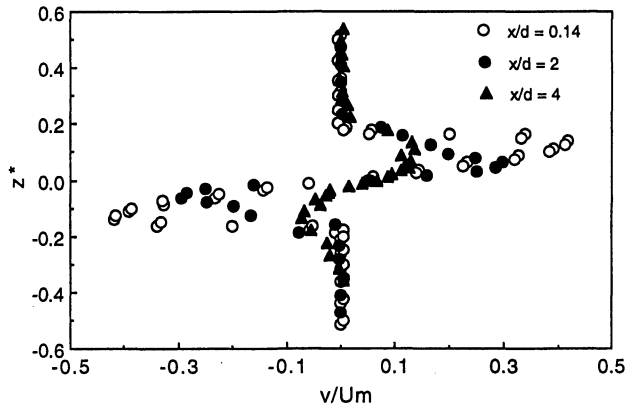

Fig. 6 Tangential velocity v/U_m vs z^* at three x/d values for $S = 0.265$ (deep mode).

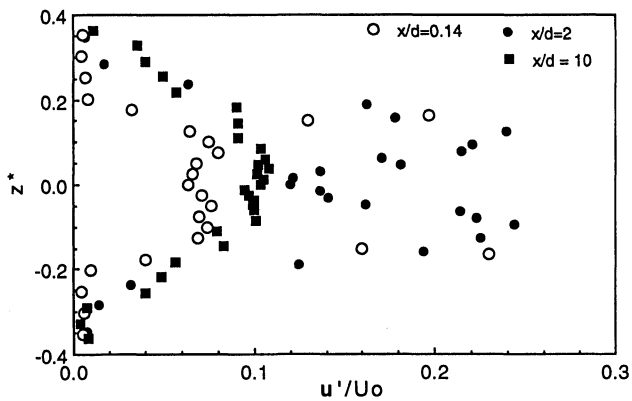

Fig. 7 RMS values of the axial velocity fluctuations u/U_0 vs z^* at three x/d values for $S = 0.265$ (deep mode).

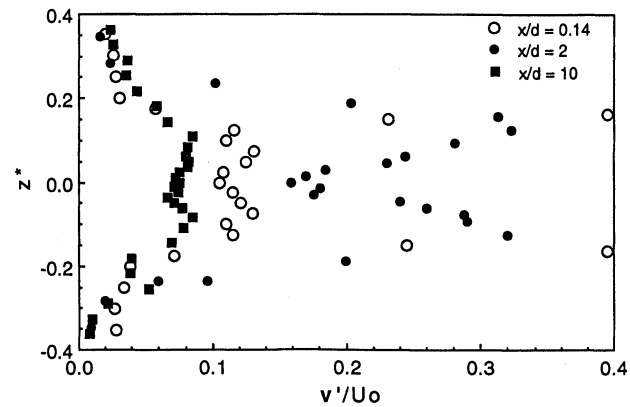

Fig. 8 RMS values of the tangential velocity fluctuations v/U_0 vs z^* at three x/d values for $S = 0.265$ (deep mode).

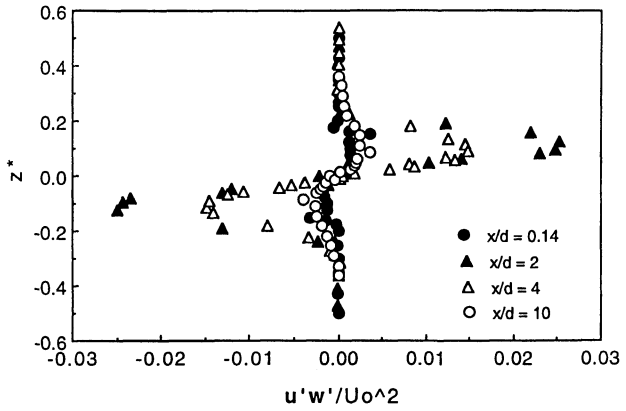

Fig. 9 Reynolds shear stress $u'w'/U_0^2$ vs z^* at four x/d for $S = 0.265$ (deep mode).

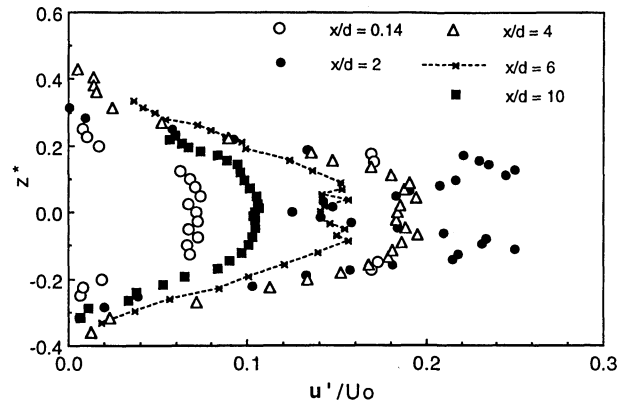

Fig. 10 RMS values of the axial velocity fluctuations u'/U_0 vs z^* at various x/d values for $S = 0.265$ (shallow mode).

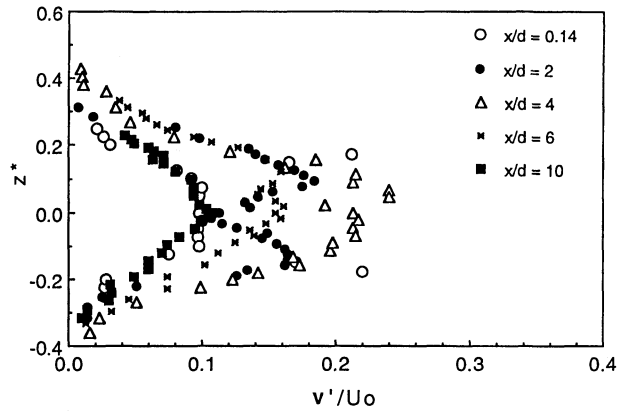

Fig. 11 RMS values of the tangential velocity fluctuations v'/U_0 vs z^* at various x/d values for $S = 0.265$ (shallow mode).

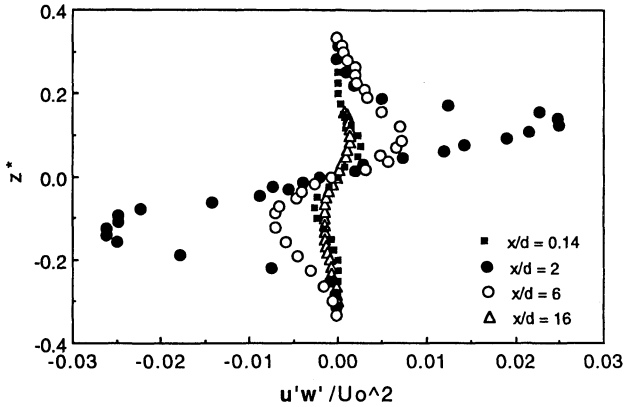

Fig. 12 Reynolds shear stress $u'w'/U_0^2$ vs z^* at four x/d values for $S = 0.265$ (shallow mode).

It is also seen that at an axial distance of as small as two diameters and beyond the axial velocity acquires a Gaussian profile, as observed by others.[18] The variation of v/U_m with z^* in Fig. 6 is such that the maximum swirl and core radius occur near the nozzle exit. Subsequently, v decreases rapidly with increasing x/d, but the decrease of the core radius beyond $x/d = 2$ is rather small. Figure 7 shows the normalized values of u' in terms of z^* only for three representative values of x/d to minimize confusion. At $x/d = 0.14$, u' is smallest in the entire cross section with the exception of the two peaks at the shear layers. At a distance of only two diameters downstream, u' jumps to its highest values and begins to spread toward the jet axis. It is also interesting to note that the maximum of u' at $x/d = 2$ is larger than the maximum of u' at $x/d = 0.14$. This shows that the shear layers are still evolving and widening. As the downstream distance increases, u' steadily decreases and becomes more Gaussian as evidenced by the case for $x/d = 10$. Figure 8 shows that the maximum of $v'(\approx 0.4)$ at $x/d = 2$ is smaller than the maximum of $v'(\approx 0.32)$ in the shear layer at $x/d = 0.14$. The reason for this is the rapid spreading of the shear layer and thus the decrease of v' along the jet axis. At $x/d = 10$, v' drops to values even lower than that which is encountered at $x/d = 0.14$. Finally, Fig. 9 shows the largest Reynolds stress ($u'w'$, the z-ward flux density of the streamwise momentum, normalized by U_0^2) at four x/d values. It increases rapidly within a distance of $2d$ and then gradually decreases toward its initial values at $x/d = 0.14$. As expected and evidenced by Figs. 5–9, the absolute values of the velocities, rms values of the velocity fluctuations, and the shear stresses, in the deep mode, are nearly symmetrical with respect to the jet axis.

Figures 10–12 show, for the shallow mode, the representative turbulence quantities at various axial distances. The vertical asymmetry of the profiles with respect to the jet axis is due to the surface proximity. In Figs. 10–12, the position of the free surface (not shown for sake of simplicity) varies with x/d, e.g., it is at $z^* = 1.12$ for $x/d = 0.14$, at $z^* = 0.27$ for $x/d = 10$, and at $z^* = 0.18$ for $x/d = 16$. A comparison of Figs. 7 (for the DM) and 10 (for the SM) shows that u'/U_0 at corresponding x/d values is nearly identical and the effect of the free surface on u'/U_0 is negligible, at least for x/d smaller than 10. However, a comparison of Figs. 8 (DM) and 11 (SM), plotted with identical horizontal scales, shows that the effect of the free surface on v'/U_0 is more complex. At smaller values of x/d (at 0.14 and 2), v'/U_0 is larger ($\approx$0.4 and 0.32, respectively) for the deep mode than for the shallow mode ($\approx$0.22 and 0.18). However, at $x/d = 10$, both modes yield nearly identical v'/U_0 values. These suggest that the lateral component of the velocity fluctuations is damped by the free surface, particularly at smaller x/d. The interfacing of the opposite-signed vorticity (of the real and image vortices) at the free surface (proximity effects) appears to be the mechanism for the said damping.[2,3,31]

The normalized values of $u'w'$ are presented in Fig. 12 for only three representative x/d values to simplify the understanding of the decay of the most important Reynolds stress. It shows that $u'w'$ acquires its largest value near $x/d = 2$, not at $x/d = 0.14$, and then decays rapidly within an additional four diameters downstream. At $x/d = 16$, $u'w'$ decreases by an order of magnitude. The other shear stresses $u'v'$ and $v'w'$ are an order of magnitude smaller than $u'w'$ at all x/d values.

Cases of Swirling Jets with $S = 0.50$ and 0.522

The discussion of results for $S = 0.50$ will be confined to $x/d = 10$ and 16 and for $S = 0.522$ to $x/d = 16$. Figure 13 shows the axial component of velocity in both the deep and shallow modes at $x/d = 10$. Clearly, it is not possible to discern any effects of the free surface at that axial distance for $S = 0.50$. The other two components (not shown here) are about an order of magnitude smaller than u.

Figure 14 ($S = 0.50$ and $x/d = 16$) shows, more emphatically than others, the effect of the free surface on the global characteristics of the swirling jet. The u component is larger for the shallow case because of the freedom of the free surface to move in an essentially shear-free environment. Figure 15 shows, for the shallow mode only, the axial, swirl, and radial components of the velocity at $x/d = 16$. The maximum of the axial velocity has drifted about $\Delta z^* \approx 0.05$ toward the free surface for reasons noted earlier. The

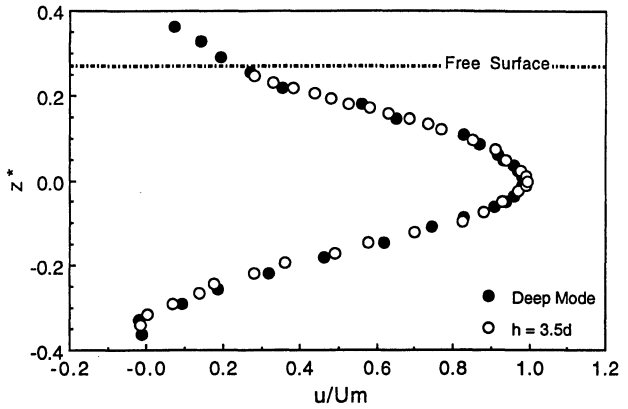

Fig. 13 Axial velocity u/U_m vs z^* at $x/d = 10$ for $S = 0.50$ (deep and shallow modes).

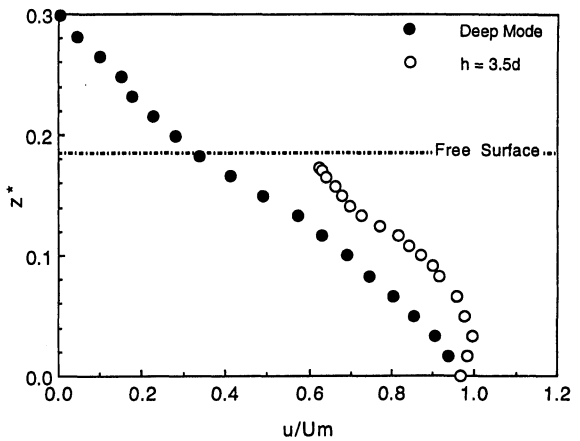

Fig. 14 Axial velocity u/U_m vs z^* at $x/d = 16$ for $S = 0.50$ (deep and shallow modes).

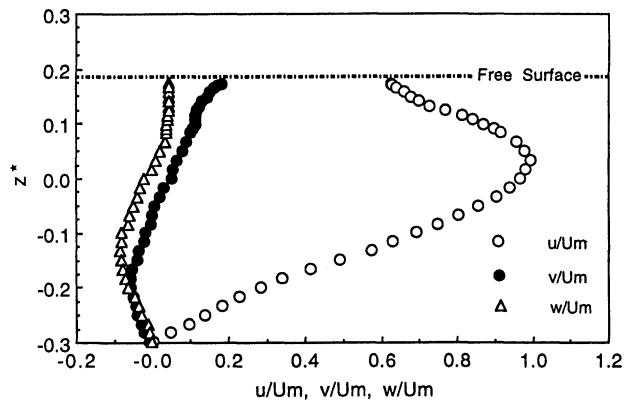

Fig. 15 RMS values of the axial, tangential, and radial velocities vs z^* at x/d = 16 for S = 0.50 (shallow mode).

swirl and radial velocities decay rapidly relative to the axial velocity. However, whereas the swirl component gradually increases toward the free surface, the radial component practically vanishes. The energy of this component is redistributed among the horizontal components.[2,3,30]

The normalized rms values of the velocity fluctuations at x/d = 16 are shown in Fig. 16. It is seen that, whereas u'/U_o and v'/U_o (open symbols) increase near the free surface, the radial or the surface normal component w'/U_o decreases continuously. This is in conformity with the previous observations and measurements.[2,3,30] Figure 17 shows the largest shear stress at $x/d = 16$ for the shallow mode. The other stresses, not shown here, are less than 10% of $u'w'/U_o^2$. Figures 16, 17, and others for smaller stresses show that the turbulence becomes increasingly anisotropic with increasing axial distance, and the stress in planes passing through the jet axis, e.g., x–z plane, increases at the expense of the stresses both in planes normal to the jet axis and in planes orthogonal to the x–z plane.

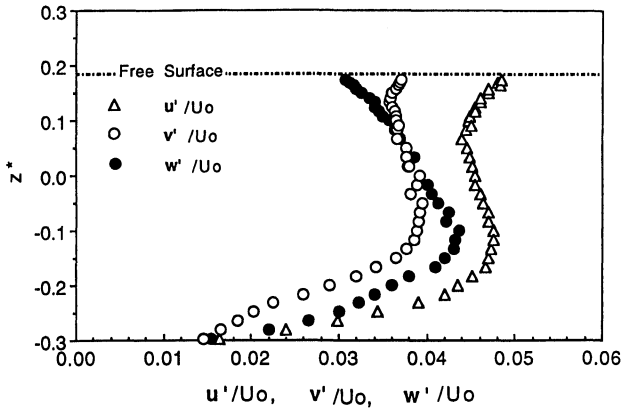

Fig. 16 Axial, tangential, and radial velocities vs z^* at x/d = 16 for S = 0.50 (deep and shallow modes).

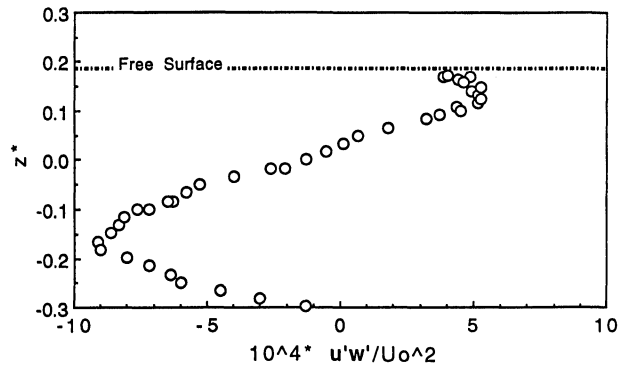

Fig. 17 Reynolds shear stress $u'w'/U_0^2$ vs z^* at x/d = 16 for S = 0.50 (shallow mode).

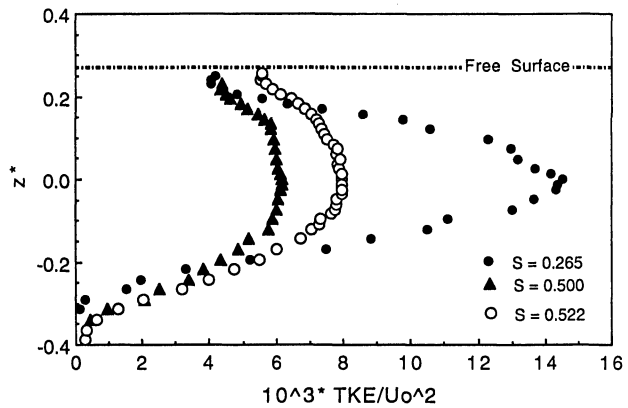

Fig. 18 TKE vs z^* at $x/d = 10$ for three swirl numbers (shallow mode).

Turbulent Kinetic Energy

Figures 18 ($x/d = 10$) and 19 ($x/d = 16$) show the normalized values of turbulent kinetic energy (TKE) for various values of S. TKE is maximum for $S = 0.265$ and decreases with increasing S for both x/d = 10 and 16. However, the decrease has two surprises. First, in either case, TKE is smallest for S = 0.50, not for S = 0.522, as one might have otherwise expected. Second, TKE for x/d = 10 becomes nearly identical for all values of S, both near the free surface and far from the free surface. For $x/d = 16$, however, TKE becomes nearly identical only for z^* smaller than about −0.15 (deeper regions). Near the free surface, TKE for $S = 0.265$ and 0.522 acquires comparable values, but for $S = 0.5$, TKE remains relatively smaller than the other two for all z^* larger than about −0.15. The fact that TKE merges near the free surface for x/d = 10 is because the free surface effects are still relatively small at $x/d = 10$ for all values of S encountered in this investigation. However, TKE for $S = 0.522$ acquiring values intermediate to those for S = 0.265 and 0.50 is a direct consequence of the creation and subsequent evolution of the swirling jet. It has been noted in connection with the discussion of

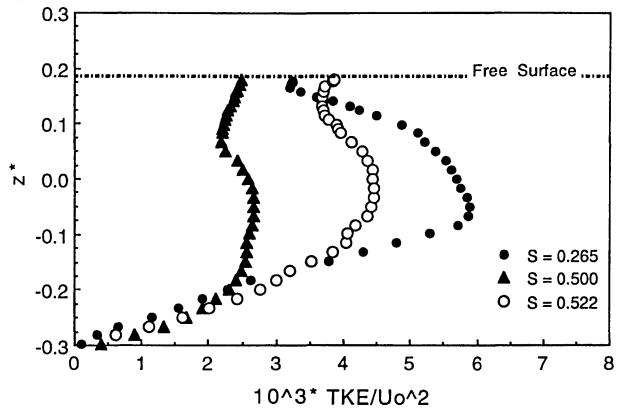

Fig. 19 TKE vs z^* at x/d = 16 for for three swirl numbers (shallow mode).

Fig. 2 that 1) for $S = 0.265$, the axial velocity decreases gradually due to the centrifugal expansion of the jet; 2) for $S = 0.50$ and 0.51, the axial velocity decreases rapidly to nearly zero and then increases to about $0.3U_0$; and 3) for S larger than about 0.51, the axial velocity begins to reverse near the nozzle exit and vortex breakdown occurs. The turbulence produced from the bursting of the vortex intensifies the turbulence within the jet and alters the velocity and turbulence distributions strongly enough to cause the surprising changes noted in TKE.

Conclusions

The turbulent flowfield created by a round swirling jet issuing from a nozzle, beneath and parallel to a free surface, in both the deep- and shallow-submergence modes, has been studied for three swirl numbers, covering the range of weak, critical, and strong swirl (S = 0.265, 0.500, and 0.522) and fixed Froude and Reynolds numbers, using a three-component LDV system. The results have shown that swirl leads to the faster spreading and quicker mixing of the jet, and the similarity of the velocity profiles is achieved at distances as close as $4d$ from the nozzle for weak ($S = 0.265$) and critical ($S = 0.50$) swirl numbers. For strongly swirling jets ($S = 0.522$), the similarity is not reached within 10 diameters downstream.

The measurements of the fluctuating components of turbulence have shown that a deeply submerged free swirling jet can be considered to be close to local isotropic turbulence except at the nozzle exit where the free shear layers are still very thin. The turbulence shear stresses exhibit anisotropic behavior, the largest always being in the plane passing through the jet axis. Stagnation occurs without vortex breakdown at a critical swirl of $S = 0.50$. For swirl numbers larger than about 0.51, vortex breakdown occurs in the jet core near the nozzle exit. The shear layer growing along the outer periphery of the jet interacts with the vortex bursting and modifies the turbulence field and leads to the production of high turbulence fluctuations.

The free surface modifies all of the foregoing characteristics of the swirling jet, particularly after a downstream distance of about $10d$, intensifies the anisotropy of the turbulence, and gives rise to complex surface structures. The change of the turbulent kinetic energy with S is not monotonic. It is maximum for $S = 0.265$, smallest for $S = 0.50$, and has an intermediate value for $S = 0.522$. This is due to the occurrence of vortex breakdown and the resulting intensification of turbulence within or near the exit of the nozzle.

The single swirling jet, with or without free-surface effects, embodies all the essential physics, without unnecessary geometric complexities, and provides ideal benchmark tests for turbulence closure models particularly because its behavior is determined more by turbulent transport than by pressure effects. The need for a robust turbulence model that can deal with the alteration of turbulence by distortion and rotation is of both scientific and practical interest and cannot be emphasized strongly enough.

Acknowledgments

This investigation has been supported by the Office of Naval Research (Contract/Grant 93WR24002). We are particularly indebted to Edwin P. Rood for his continuous guidance and encouragement.

References

[1]Munk, W. H., Scully-Power, P., and Zachariasen, F., "Ship Wakes from Space: The Bakerian Lecture," *Proceedings of the Royal Society of London A*, Vol. 412, Aug. 1987, pp. 231–254.

[2]Sarpkaya, T., and Suthon, P., "Interaction of a Vortex Couple with a Free Surface," *Experiments in Fluids*, Vol. 11, No. 11, 1991, pp. 205–217.

[3]Sarpkaya, T., "Vorticity, Free Surface and Surfactants," *Annual Review of Fluid Mechanics*, Vol. 28, 1996, pp. 83–128.

[4]Gupta, A. K., Lilley, D. G., and Syred, N., *Swirl Flows*, Abacus, Tunbridge Wells, England, UK, 1984, pp. 1–100.

[5]Rhode, D. L., Lilley, D. G., and McLaughlin, D. K., "On the Prediction of Swirling Flowfields Found in Axisymmetric Combustor Geometries," *Journal of Fluids Engineering*, Vol. 104, Sept. 1982, pp. 378–384.

[6]Wu, C., and Farokhi, S., "Spatial Instability of a Swirling Jet-Theory and Experiment," *AIAA Journal*, Vol. 30, No. 6, 1992, pp. 1545–1552.

[7]Sarpkaya, T., "Trailing Vortices in Homogeneous and Density-Stratified Media," *Journal of Fluid Mechanics*, Vol. 136, Nov. 1983, pp. 85–109.

[8]Sarpkaya, T., and Daly, J. J., "Effect of Ambient Turbulence on Trailing Vortices," *Journal of Aircraft*, Vol. 26, No. 6, 1987, pp. 399–404.

[9]Devenport, W. J., Rife, M. C., Liapis, S. I., and Follin, G. J., "The Structure and Development of a Wing-Tip Vortex," *Journal of Fluid Mechanics*, Vol. 312, April 1996, pp. 67–106.

[10]Launder, B. E., and Morse, A. P., "Numerical Prediction of Axisymmetric Free Shear Flows with a Reynolds Stress Closure," *Turbulent Shear Flows I*, edited by F. Durst, F. W. Schmidt, and J. H. Whitelaw, Vol. 1, Springer–Verlag, Berlin, 1979, pp. 279–294.

[11]Morse, A. P., "Axisymmetric Turbulent Shear Flows With and Without Swirl," Ph.D. Thesis, Civil Engineering Dept., Univ. of London, London, 1980.

[12]Abujelala, M. T., and Lilley, D. G., "Limitations and Empirical Extensions of the k-ε Model as Applied to Turbulent Confined Swirling Flows," *Chemical Engineering Communications*, Vol. 31, May 1984, pp. 223–236.

[13]Gibson, M. M., and Younis, B. A., "Calculation of Swirling Jets with a Reynolds Stress Closure," *Physics of Fluids*, Vol. 29, No. 1, 1986, pp. 38–48.

[14]Younis, B. A., Gatski, T. B., and Speziale, C. G., "Assessment of the SCG Pressure-Strain Model in Free Turbulent Jets With and Without Swirl," *Journal of Fluids Engineering*, Vol. 118, Dec. 1996, pp. 800–809.

[15]Speziale, C. G., Gatski, T. B., and MacGiolla Mhuiris, N., "A Critical Comparison of Turbulence Models for Homogeneous Shear Flows in a Rotating Frame," *Physics of Fluids*, Vol. 2, No. 9, 1990, pp. 1678–1684.

[16]Cambon, C., "Turbulent Flows Undergoing Distortion and Rotation," *Fluid Dynamics Research*, Vol. 13, No. 6, 1994, pp. 281–298.

[17]Hossain, M., "Reduction in the Dimensionality of Turbulence due to a Strong Rotation," *Physics of Fluids*, Vol. 6, No. 3, 1994, pp. 1077–1080.

[18]Chigier, N. A., and Chervinsky, A., "Experimental Investigation of Swirling Vortex Motion in Jets," *Journal of Applied Mechanics*, Vol. 34, June 1967, pp. 443–451.

[19]Farokhi, S., Taghavi, R., and Rice, E. J., "Effect of Initial Swirl Distribution on the Evolution of a Turbulent Jet," *AIAA Journal*, Vol. 27, No. 6, 1989, pp. 700–706.

[20]Rose, W. G., "A Swirling Round Turbulent Jet: 1-Mean-Flow Measurements," *Journal of Applied Mechanics*, Vol. 29, Dec. 1962, pp. 615–625.

[21]Pratte, B. D., and Keffer, J. F., "The Swirling Turbulent Jet," *Journal of Basic Engineering*, Vol. 93, Dec. 1972, pp. 739–748.

[22]Hallett, W. L. H., and Toews, D. J., "The Effects of Inlet Conditions and Expansion Ratio on the Onset of Flow Reversal in Swirling Flow in a Sudden Expansion," *Experiments in Fluids*, Vol. 5, No. 2, 1987, pp. 129–133.

[23]Kihm, K. D., Chigier, N., and Sun, F., "Laser Doppler Velocimetry Investigation of Swirler Flowfields," *Journal of Propulsion and Power*, Vol. 6, No. 4, 1990, pp. 364–373.

[24]Panda, J., and McLaughlin, D. K., "Experiments on the Instability of a Swirling Jet," *Physics of Fluids*, Vol. 6, No. 1, 1994, pp. 263–276.

[25]Stevenson, W. H., Thompson, H. D., and Roesler, T., "Direct Measurement of Laser Velocimeter Bias Errors in a Turbulent Flow," *AIAA Journal*, Vol. 20, No. 12, 1982, pp. 1720–1723.

[26]McLaughlin, D., and Tiederman, W., "Biasing Correction for Individual Realization Laser Anemometer Measurements in Turbulent Flows," *Physics of Fluids*, Vol. 16, Dec. 1973, pp. 2082–2088.

[27]Moffat, R. J., "Contributions to the Theory of Single-Sample Uncertainty Analysis," *Journal of Fluids Engineering*, Vol. 104, June 1982, pp. 250–260.

[28]Sarpkaya, T., "On Stationary and Traveling Vortex Breakdowns," *Journal of Fluid Mechanics*, Vol. 45, March 1971, pp. 545–559.

[29]Sarpkaya, T., "Turbulent Vortex Breakdown," *Physics of Fluids*, Vol. 7, No. 10, 1995, pp. 2301–2303.

[30]Batchelor, G. K., *An Introduction to Fluid Dynamics*, Cambridge Univ. Press, Cambridge, England, UK, 1967, pp. 543–550.

[31]Sarpkaya, T., and Neubert, D., "Interaction of a Streamwise Vortex with a Free Surface," *AIAA Journal*, Vol. 32. No. 3, 1994, pp. 594–600.

F. W. Chambers
Associate Editor